Passive Localization Through Channel Estimation of On-the-Air LTE Signals

YAFEI TIAN[ID], **(Member, IEEE), YANGYANG HE, AND HAO DUAN**

School of Electronics and Information Engineering, Beihang University, Beijing 100191, China

Corresponding author: Yafei Tian (ytian@buaa.edu.cn)

ABSTRACT Wireless communication signal is a kind of coherent illuminator, and it can shed light on surrounding environments. The mobile terminal receives the signal and estimate the propagation channel, and can sense the moving objects passively. The localization module and communication module share the RF front-end and baseband processing, and thus greatly reduce the implementation cost in mobile terminals. Passive localization is based on the delay estimation of the dynamic reflection path. However, several practical factors prohibit the accurate estimation of the propagation delays. The multipath reflection and scattering are abundant in urban and indoor environments, and the signal bandwidth is usually not large enough to reach a fine delay resolution. The synchronization error, sampling clock drift, frequency offset and phase noise will severely impact the estimation performance. In this article, we propose a set of methods to make the practical application of this method possible. We also derive the Cramer-Rao lower bound of the delay estimation, and analyze the estimation error related with various impact factors. A prototype system is built to test the performance in real environments, and various experiments have been done to verify its feasibility. We believe that the fusion of wireless communication and sensing is a potential enhancement of next generation cellular system, and the capability of passive location will bring interesting applications for smart phones.

INDEX TERMS Cramer-Rao bound, delay estimation, external illuminator, passive localization, super-resolution analysis.

I. INTRODUCTION

Wireless communication signals not only carry the information of data but also encode the information of propagation channels [2]. On the signal propagation path, the variations of reflection, scattering, and diffraction will affect the channel response. Through analyzing the acquired channel state information (CSI), we can sense the environment changes, such as detecting the moving object, localizing its position, or following its trajectory, whereas it is not required for the object to carry any device on it [3]. Wireless sensing can be used as a personal radar for intruder detection, or be used as a human-computer interaction interface for gesture recognition [4]. It also has potential applications in e-Health, such as fall detection and real-time assistance for older adults [5].

Many kinds of wireless signals have been used as external illuminators, e.g., cellular, Wi-Fi, DAB/DVB, RFID, and even GPS signals [6], [7]. Among these sources, Wi-Fi signal

is most widely used, since there is commodity network card that the channel state information (CSI) can be extracted easily from the drivers [8].

A "WiSee" system was demonstrated in 2013 and has attracted a lot of attention [9]. By analyzing the variation of Doppler shift of the received Wi-Fi signal, it can distinguish nine human gestures moving indoors. In [10], a "WiHear" system is proposed, which can detect channel changes caused by mouth movement in the case of non-line of sight, so as to listen to people's conversation. In [11], an "RT-Fall" system is proposed, which can detect human falls comparing with other daily movement at home. A "BreathTrack" system is proposed in [12], through calibration by the hardware and software joint corrections, the phase variation of the CSI is tracked to estimate the human breath rate. A device-free human identification system is proposed in [13], the intrinsic features such as respiration and gait are extracted from the CSI to identify different peoples.

Wi-Fi signal is not continuously transmitted. When there is a service requirement, there is a burst of data payload.

The time intervals among the packets are random, thus there will be a random initial phase for the synchronization of each packet. In [14] and [15], the CSI correlation matrices are used to do moving human detection. Through-the-wall detection is studied in [16], since the line-of-sight (LOS) signal and static reflected signal by the wall is much stronger than the reflection after the wall, eigenvalue analysis at each subcarrier are executed and the difference of the eigenvectors are extracted as feature vectors. However, these works only find the existence or not of a moving human, there is no location information provided.

Radio and television signals can also be used as external illuminators. Since these kind of radiation sources have high power, we can use them to find distant targets [17], [18]. The passive radar system usually uses two receivers working simultaneously, which may have different beam width, direction and amplifier gain. One receiver is used to receive the reference signal and the other is used to monitor the target echo. By comparing the reference signal and the surveillance signal, range and Doppler information of the target can be extracted. The digital audio broadcasting signal (DRM) is used in [19]. Since the high frequency (HF) signal transmits over-the-horizon in the form of sky wave ionospheric reflection, the passive receiver can monitor the airspace over a range of 2000 kilometers. The digital TV signals (DTMB) from multiple TV stations are used in [20]. Since the DTMB stations transmit the same signal at the same frequency, it is difficult to distinguish the reflected signals of the same target from those of different transmitters. Moreover, demodulating and reconstructing the reference signal bring great burden of computation and delay. In [21], OFDM waveform is investigated and the range and Doppler parameters are directly estimated from the channel estimation. However, if the target is close to the terminal and moves slow, as of a human walks at home, the conventional range-Doppler detection mode will fail.

In urban and indoor environments, non-line-of-sight (NLOS) propagation and multipath reflections will cause severe localization error. Using a signal with ultra-wideband (UWB) will partly relieve this influence, since UWB signal has fine delay resolution and can distinguish the reflective paths of close objects. Passive localization of the reflectors using UWB signal is studied in [22], [23], where multiple distributed transmitters and receivers are used. The propagation delays between each pair of transceivers are measured, including direct path and all reflection paths, and then the propagation delays of the same reflector from the measurements of multiple pairs of transceivers are correlated to determine its position. However, the transmit power of UWB signal is restricted and there is spectrum regulation problem in many countries, it is difficult to integrate into the existing mobile terminal architecture.

Back to the narrow band signal with a carrier, in [24] the interference principle in optics is borrowed to explain the phenomenon happened between the reflected signal of a moving object and that of stationary objects. When the propagation distance of the reflection path changes one wavelength, the carrier phase of the dynamic reflection signal changes 2π, the interferenced waveform changes one period. In fact, the concepts of signal interference effect and Fresnel zone have been deeply studied in the field of wireless communication [25]. However, in recent years, we have been accustomed to interpreting this interference effect as "random" superposition between multipath signals, considering small-scale fading of channels as random variables of Rayleigh or Rice distribution. We have overlooked the deterministic aspects of the time-varying channel response that can be analyzed with certainty.

While Wi-Fi signal distributes widely in homes and office buildings, LTE signal has seamless coverage in all the cities and most of the rural areas. Besides, LTE base station has non-stop broadcasting of the cell-specific reference signals (CRS) so that we can acquire continuous channel estimation. In [26], the device-free motion detection via LTE signal is tested in real environments, where the amplitude fluctuation and phase variation of the channel response are used as the judgment basis. According to the reflection or scattering models, the discovery region can be determined by the reflective strength. In [27], exploiting LTE base stations as illuminators of opportunity, a Bayesian framework for tracking mobile targets and estimating their velocity has been developed. In practice, it has another advantage to use LTE signal for passive localization. Since the communication module also need to do channel estimation, the localization module can reuse the channel estimation results without requirement of a separate RF front-end, thus can greatly reduce the implementation cost and power consumption of wireless sensing in mobile terminals.

Passive localization starts from the estimation of the propagation delay of the dynamic reflection path, where one value of the delay will determine an ellipse given the positions of the transmitter and receiver as two focal points. After obtaining a group of delay estimations from multiple pairs of transmitters and receivers, we can calculate the intersection point of these ellipses as the localization result. However, the estimation accuracy is usually limited by many practical imperfections. The multipath reflection and scattering are abundant in urban and indoor environments, and the signal bandwidth is usually not large enough to reach a fine delay resolution. The reflections by human bodies and arms are weak. The synchronization error, sampling clock drift, frequency offset and phase noise will severely impact the estimation performance. In this paper, we design a preprocessing method to compensate the frequency offset and separate the weak dynamic reflection path from the strong direct and static reflection paths. We apply the super-resolution method to estimate the delay of the dynamic path, and apply the sparse optimization method to estimate the delays of the static paths. The impact of synchronization error, sampling clock drift and phase noise are removed. We also derive the Cramer-Rao lower bound (CRLB) of the delay estimation, and analyze the estimation error depending on various impact factors.

A prototype system is built to test the performance in real environments, and various experiments have been done to verify its feasibility.

The main contributions of this paper are in the following four aspects:

1) we introduce a system model that incorporating the propagation environment, target characteristic, and transceiver imperfections, so that build the relationship between the channel response and the target location;

2) we design the preprocessing method to compensate the frequency offset and separate the dynamic and static paths, and design the delay estimation methods with the impact of phase noise;

3) we derive the Cramer-Rao lower bound of the delay estimation, and analyze the estimation error related with the reflection strength, signal bandwidth, integration time and path distance differences;

4) we implement a prototype to work in real environments, and carry on various experiments to test its performance.

The rest of this paper is organized as follows. In Section II, we introduce the system model. In Section III, we propose the preprocessing method and the delay estimation methods of the dynamic and static paths, and constitute the complete passive localization algorithm. In Section IV, CRLB is derived and different factors that impacting on the system performance are analyzed. In Section V, the prototype implementation and experiment results are demonstrated. Finally, Section VI concludes the paper.

II. SYSTEM MODEL

For the propagation of wireless communication signals, except of LOS channel, there are multipaths caused by reflection, refraction, diffraction, and scattering. When there is a moving object appear in the propagation environment, there will be a dynamic path reflected or scattered by this object, and the dynamic reflection signal will combine with other static reflection signals at the receiver antenna. The channel response is composed of the amplitude, phase and delay of every path, and is impacted by the synchronization error, sampling clock drift, frequency offset and phase noise as well. If we can correctly estimate the propagation delay of the dynamic reflection path, we can localize the position of that reflective object by triangular method using information from several pairs of transceivers.

A. CHANNEL MODEL

The channel response estimated in the receiver is the superposition of the static reflection paths and the dynamic reflection path caused by the moving target. When the moving object changed its position, the sum distance from the transmitter to the target and from the target to the receiver will change accordingly. This will change the amplitude and phase of the channel response of the reflection path, and will certainly change the overall channel response. As shown in Fig. 1, at time t, when the sum distance between the target and transceivers is $d_i(t)$, the received baseband signal can be
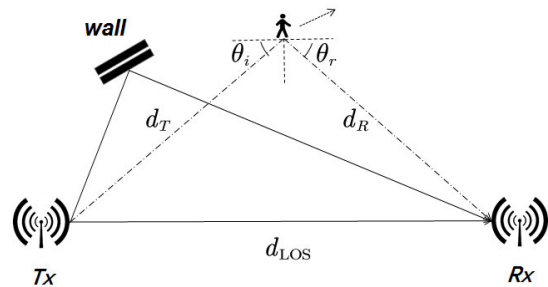

FIGURE 1. Typical scenario of multipath propagation.

expressed as

$$r(t) = \sum_{l=1}^{L} a_l e^{-j\omega_c \frac{d_l}{c}} s\left(t - \frac{d_l}{c}\right)$$
$$+ a_i(t) e^{-j\omega_c \frac{d_i(t)}{c}} s\left(t - \frac{d_i(t)}{c}\right) + n(t), \quad (1)$$

where $s(t)$ is the baseband transmit signal, c is the light speed, $\omega_c = 2\pi f_c$ and f_c is the carrier frequency. The wavelength of the carrier is $\lambda = c/f_c$. The summation of L signals in the first term of the right side represents the summation of signals from the direct path and all other static reflection paths, and a_l is the channel gain of the l-th path. The second term of the right side is the signal reflected from the moving object. When $d_i(t)$ changes within several wavelengths, the variation of channel gain $a_i(t)$ and propagation delay $d_i(t)/c$ can be omitted. The significant variation is only the carrier phase $2\pi d_i(t)/\lambda$. For simplicity, we only consider the single-hop reflection as the dynamic path, since the multi-hop reflections would be too weak to be separated.

The amplitude of the reflection path $a_i(t)$ depends on the large-scale path loss and the reflective features of the moving object. If the surface of the object is large and smooth relative to the wavelength, and the positions of Tx, Rx and the moving object agree with the reflection law, the specular reflection effect will be dominant in the received power [25], i.e.,

$$P_R = P_T + 20 \log \frac{\Gamma_r \lambda}{4\pi (d_T + d_R)}, \quad (2)$$

where P_T denotes transmit power, and Γ_r is the reflective coefficient that depends on the incident angle θ_i, the relative permittivity of the material ϵ_r, and the polarization of the electromagnetic wave. For perpendicular polarization (E-field not in the plane of incidence),

$$\Gamma_r = \frac{\sin \theta_i - \sqrt{\epsilon_r - \cos^2 \theta_i}}{\sin \theta_i + \sqrt{\epsilon_r - \cos^2 \theta_i}}, \quad (3)$$

and for parallel polarization,

$$\Gamma_r = \frac{-\epsilon_r \sin \theta_i + \sqrt{\epsilon_r - \cos^2 \theta_i}}{\epsilon_r \sin \theta_i + \sqrt{\epsilon_r - \cos^2 \theta_i}}. \quad (4)$$

From (2), we can see that in this situation the large-scale path loss depends on the sum of d_T and d_R.

Otherwise, the scattering effect is dominant. The received power will be determined by the radar cross section (RCS) of the object [25], i.e.,

$$P_R = P_T + 20\log\frac{\lambda}{d_T d_R} + RCS - 30\log(4\pi),\quad (5)$$

where RCS is in units of dB·m^2 and is related with the surface area and scattering characteristic of the object. Note that in this situation the large-scale path loss depends on the product of d_T and d_R.

In both cases, $a_i(t)$ can be calculated as

$$a_i(t) = 10^{\frac{P_R - P_T}{20}}.\quad (6)$$

From the measurement results in [26], in most cases the scattering model is more preferable. After all, the reflective law is hard to be kept when the human moves naturally.

When there are multiple moving objects in the environment, there are multiple dynamic reflections, the received signal is then

$$r(t) = \sum_{l=1}^{L} a_l e^{-j\omega_c \tau_l} s(t - \tau_l)$$
$$+ \sum_{i=1}^{K} a_i e^{-j\omega_c \tau_i(t)} s(t - \tau_i(t)) + n(t),\quad (7)$$

where the time delay $d_i(t)/c$ is substituted by $\tau_i(t)$. Assuming the bandwidth of the baseband signal is B, it is worth to note that the time delay resolution in the time domain is $1/B$. When the delay difference between two reflection paths is less than $1/B$, it is hard to recognize them as two distinct paths. For example, an LTE signal has a bandwidth of 20 MHz, its delay resolution is 50 ns.

For LTE signal, we can use CRS to do channel estimation. In each subframe that with 1 ms duration, there are four OFDM symbols that contains CRS, and for 20 MHz bandwidth configuration, in each symbol there are 200 subcarriers occupied by CRS.

From the received signal, we can estimate the channel state information (CSI) through the known CRS subcarriers. Since the propagation channel is composed by the direct path, static reflection paths, and the dynamic reflection paths, the CSI can be separated into two parts, i.e., the static part and dynamic part, as shown in the following,

$$H(\omega, t) = \sum_{l=1}^{L} a_l e^{-j\omega_c \tau_l} e^{-j\omega \tau_l}$$
$$+ \sum_{i=1}^{K} a_i(t) e^{-j\omega_c \tau_i(t)} e^{-j\omega \tau_i(t)} + n(\omega, t)$$
$$= H_s(\omega) + H_d(\omega, t) + n(\omega, t),\quad (8)$$

where ω is the angular frequency of the baseband subcarriers, $H_s(\omega)$ is the static channel response and $H_d(\omega, t)$ is the dynamic channel response, $n(\omega, t)$ is the received noise.

B. THE EFFECT OF NON-IDEAL FACTORS

In practical system, there are synchronization error, sampling clock drift, frequency offset and phase noise. Considering these factors, the baseband received signal will be

$$r(t) = e^{j[\omega_d t + \phi(t)]} \left\{ \sum_{l=1}^{L} a_l e^{-j\omega_c \tau_l'(t)} s[t - \tau_l'(t)] \right.$$
$$\left. + \sum_{i=1}^{K} a_i e^{-j\omega_c \tau_i'(t)} s[t - \tau_i'(t)] \right\} + n(t),\quad (9)$$

where ω_d is the frequency offset, $\phi(t)$ is the phase noise. The delays τ_l' and τ_i' are affected by the synchronization error Δ and the sampling clock drift $\delta(t)$, i.e.,

$$\tau_l'(t) = \tau_l + \Delta + \delta(t),$$
$$\tau_i'(t) = \tau_i(t) + \Delta + \delta(t).\quad (10)$$

The drifting speed of the sampling clock is not neglectable comparing with the the variation speed of τ_i. For example, if a human moves with a speed of 1 m/s, the delay τ_i changes within 6.6 ns per second. Whereas the clock drift is 10 ns per second if a very high quality crystal oscillator is used (assuming its frequency stability is 0.01 ppm). Nowadays, however the frequency stability of commodity communication modules is often in between 1 ppm to 10 ppm. The clock drift can be as large as 10 us in one second.

Correspondingly, the channel estimation result is affected by these non-ideal factors

$$H'(\omega, t) = e^{j[\omega_d t + \phi(t)]} \left\{ \sum_{l=1}^{L} a_l e^{-j\omega_c \tau_l'(t)} e^{-j\omega \tau_l'(t)} \right.$$
$$\left. + \sum_{i=1}^{K} a_i(t) e^{-j\omega_c \tau_i'(t)} e^{-j\omega \tau_i'(t)} \right\} + n(\omega, t)$$
$$= e^{j[\omega_d t + \phi(t)]} \{ H_s'(\omega, t) + H_d'(\omega, t) \} + n(\omega, t).\quad (11)$$

In the process of delay estimation, we must explore various methods to eliminate the impact of these factors.

C. LOCALIZATION MODEL

From (10) we can see that, in the delay estimation of the static and dynamic paths, the bias terms caused by synchronization error and sampling clock drift are same, i.e.,

$$\tau_i(t) - \tau_l = \tau_i'(t) - \tau_l'(t).\quad (12)$$

Thus the propagation delay of the i-th reflection path can be calculated as

$$\tau_i(t) = \tau_0 + (\tau_i'(t) - \tau_0'(t)),\quad (13)$$

where τ_0 is the real propagation delay of the direct path, τ_0' is the estimated delay of the direct path. The true value of τ_0 is calculated by the known positions of the transmitter and receiver, where the position of base station is fixed and can be provided by the telecommunication carrier, and the position of mobile terminal is obtained by existed techniques such
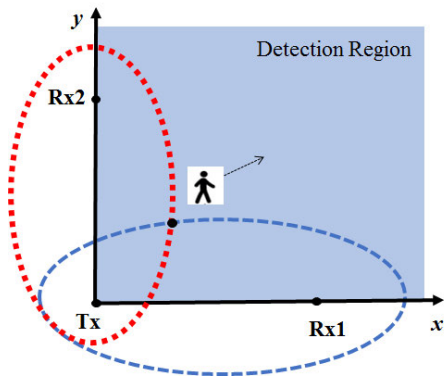
FIGURE 2. The localization model.

as satellite and innertial navigations, or localization through cellular or Wi-Fi signals.

In practice, there might be obstacles between the transmitter and receiver and the direct path is too weak. In this case, we will try to find the first arrived path, no matter its strength. However, for the estimation of τ_0', if the estimated first arrived path is a static reflection path rather than the direct path, there will be extra estimation error.

Once the propagation delay of the *i*-th reflection path is estimated, the propagation distance of that path is known, and we can determine an ellipse given the positions of transmitter and receiver as two focal points. The sum distance from the transmitter and receiver to the *i*-th moving object just equals to the long axis of the ellipse. If we have two pairs of transceivers, we can use two ellipses determining a crossover point, which is the location of the moving object. The localization model is shown in Fig. 2.

Usually there are multiple base stations available for an LTE terminal to be listened to, although their signal strength might be different. Passive localization of the moving target can be achieved for a terminal with only one antenna. If one terminal is equipped with multiple distributed antennas (e.g., for some specified equipment), or multiple terminals can exchange their delay estimations, we can obtain more precise localization results. In this paper, however, we mainly study the delay estimation problem of one transceiver pair. The problems of localization with multiple transceiver pairs and tracking with consecutive delay estimations will be studied in future topics.

III. DELAY ESTIMATION ALGORITHM

To remove the impact of synchronization error and sampling drift, we need simultaneously estimate the propagation delays of the dynamic path and the direct path. Each dynamic path has independent fast changing phase, and the channel responses of multiple dynamic paths are superimposed together. Thus the delay estimation of dynamic paths belongs to the line spectra estimation problem, and we can use classic super-resolution algorithm to estimate them. The channel responses of static paths are also superimposed, they are usually non-distinguishable due to the limited bandwidth,

and in a short duration the amplitudes and phases can be seemed as fixed. Thus we use optimization-based algorithm to solve this problem. Of course, some preprocessings on the channel estimations are required for the first step. We will compensate the frequency offset and separate the dynamic and static channel responses.

A. PREPROCESSINGS

From (11), we know that the channel estimation values are impacted by the frequency offset ω_d and phase noise $\phi(t)$. Actually, there is frequency synchronization along with the frame synchronization. But there must be estimation error for the frequency offset, thus we can regard ω_d as the residual frequency offset after the frequency synchronization.

A phase locked loop (PLL) is applied to track the phase. From (11) we can see that, except the frequency offset and phase noise, each path has a changing phase. We will first transform the channel responses from the frequency domain to time domain, and then track the strongest path in time domain. The strongest path is either the direct path or a strong reflection path, its phase term $\omega_c \tau_l'(t)$ only changes with the timing drift $\delta(t)$. This kind of changing is slow and can be tracked. Meanwhile, the phase changes of the dynamic path can be kept.

The PLL is a low-pass filter applied on the phase. The frequency offset and the low-frequency components in the phase noise can thus be compensated. However, the high-frequency components in the phase noise are still left. We denote this residual phase noise as $\phi'(t)$, with zero mean and variance σ_ϕ^2. This residual phase noise is very small, and it usually does not cause any harm to communication systems. However, through practical experiments we find that its impact on the delay estimation problem is serious and must be taken care of. The channel response is thus expressed as

$$H''(\omega, t) = e^{j\phi'(t)} \left\{ \sum_{l=1}^{L} a_l e^{-j\omega_c \tau_l} e^{-j\omega \tau_l'(t)} \right.$$
$$\left. + \sum_{i=1}^{K} a_i(t) e^{-j\omega_c \tau_i(t)} e^{-j\omega \tau_i'(t)} \right\} + n(\omega, t)$$
$$= e^{j\phi'(t)} [H_s''(\omega, t) + H_d''(\omega, t)] + n(\omega, t). \quad (14)$$

Note that the impact of $\Delta + \delta(t)$ is removed from the phase terms due to phase tracking, but it cannot be removed from the delay.

After phase tracking, we need separate the channel response into dynamic part and static part, and then estimate the corresponding delays respectively. Compared with the static reflections, the strength of dynamic reflections generated by the moving objects are usually much lower. The static reflections are usually generated by buildings, walls or furniture. But the moving object are usually human bodies, arms, or even fingers. The RCSs of these objects are usually small. Thus the SNR of the dynamic channel response is much lower than the static channel response. If we estimate

the delays of dynamic paths without separation, the static paths will behave as strong interferences.

We design a low pass filter to first separate the static channel response, that is

$$\hat{H}_s(\omega, t) = \mathcal{F}_{LP}\{H''(\omega, t)\} \approx H''_s(\omega, t), \tag{15}$$

where $\mathcal{F}_{LP}\{\cdot\}$ is a low pass filter. It can be implemented by a moving average window, and the window length will control the cutoff frequency. Since the mean value of $\phi'(t)$ is 0 and $\phi'(t)$ is very small, the mean value of $e^{j\phi'(t)}$ is 1.

The dynamic channel response can then be separated as

$$\begin{aligned}
\hat{H}_d(\omega, t) &= H''(\omega, t) - \hat{H}_s(\omega, t) \\
&= [e^{j\phi'(t)} - 1]H''_s(\omega, t) + e^{j\phi'(t)}H''_d(\omega, t) + n(\omega, t) \\
&\approx j\phi'(t)H''_s(\omega, t) + H''_d(\omega, t) + n(\omega, t),
\end{aligned} \tag{16}$$

where the approximation is because that $\phi'(t)$ is very small. Since the magnitude of $H''_s(\omega, t)$ is possible to be much larger than that of $H''_d(\omega, t)$, for example 1000 times, the term $j\phi'(t)H''_s(\omega, t)$ is not neglectable.

B. DELAY ESTIMATION OF DYNAMIC PATHS
In this part, we first estimate the delays of the dynamic paths, $\tau'_i(t)$. From (14), we know that the channel response of dynamic paths is

$$\begin{aligned}
H''_d(\omega, t) &= \sum_{i=1}^{K} a_i(t)e^{-j\omega_c\tau_i(t)}e^{-j\omega\tau'_i(t)} \\
&= \sum_{i=1}^{K} g_i(t)e^{-j\omega\tau'_i(t)},
\end{aligned} \tag{17}$$

where $g_i(t)$ denote the complex coefficient of the i-th dynamic path. Since the carrier frequency ω_c is much higher than the baseband frequency ω, in a short duration (such as 100 ms), the term $\omega_c\tau'_i(t)$ is variant but the term $\omega\tau'_i(t)$ can be seemed as a constant (only depends on ω). We consider the real-time estimation problem that outputting the delay estimation results slot by slot, where in each slot the fixed parameter assumption is satisfied.

At each time instance t, the channel responses at different subcarrier form a vector

$$\boldsymbol{h}'_d(t) = \begin{bmatrix} e^{-j\omega_1\tau'_1} & e^{-j\omega_1\tau'_2} & \cdots & e^{-j\omega_1\tau'_K} \\ e^{-j\omega_2\tau'_1} & e^{-j\omega_2\tau'_2} & \cdots & e^{-j\omega_2\tau'_K} \\ \vdots & \vdots & \ddots & \vdots \\ e^{-j\omega_N\tau'_1} & e^{-j\omega_N\tau'_2} & \cdots & e^{-j\omega_N\tau'_K} \end{bmatrix} \begin{bmatrix} g_1(t) \\ g_2(t) \\ \vdots \\ g_K(t) \end{bmatrix}, \tag{18}$$

where ω_1 to ω_N are the know baseband frequency, τ'_1 to τ'_K are parameters to be estimated.

From (16) we know that, there are also two interference terms in the separated dynamic channel responses, where $n(\omega, t)$ is circularly symmtric white Gaussian noise, and $j\phi'(t)H''_s(\omega, t)$ is the frequency-domain channel response of the static paths multiplied by the residual phase noise.

The separated dynamic channel response can also be written in vector form, i.e.,

$$\hat{\boldsymbol{h}}_d(t) = \boldsymbol{h}'_d(t) + \boldsymbol{n}'(t), \tag{19}$$

where the covariance matrix of $\boldsymbol{n}'(t)$ is

$$\boldsymbol{\Gamma} = \sigma_\phi^2 E\{\boldsymbol{h}'_s(t)\boldsymbol{h}'^H_s(t)\} + \sigma^2 \boldsymbol{I}. \tag{20}$$

The estimation of delay τ'_i, $i = 1, \ldots, K$, is a line spectra estimation problem [28]. We will apply the classical super-resolution estimation method, i.e., estimating signal parameters via rotational invariance techniques (ESPRIT), to solve it. The ESPRIT algorithm is oriented from array signal processing. When the receiver is equipped with an antenna array, we can separate the array into two equal-size subarrays. The offsets of the corresponding antenna elements in two subarrays are the same, that means, for a given incident angle the differences of the propagation distances to the elements of two subarrays are the same. The propagation distance difference corresponds to a phase difference for the received signal, and the phase difference is called a rotational invariance factor. Through solving a generalized eigen-value equation, the incident angle can be estimated.

For our delay estimation problem, the rotational factor can be constructed from the multiple subcarriers structure. We can form two subarrays with fixed subcarrier spacing, and these two subarrays are related by a rotational factor matrix. The delay information can be estimated from the rotational factor matrix.

Concretely, after we get the estimation of the dynamic channel response $\hat{\boldsymbol{h}}_d(t)$, two vectors $\boldsymbol{x}_1(t)$ and $\boldsymbol{x}_2(t)$ can be constructed by extracting the elements in even and odd subcarriers, respectively, i.e.,

$$\begin{aligned}
\boldsymbol{x}_1(t) &= \begin{bmatrix} e^{-j\omega_1\tau'_1} & \cdots & e^{-j\omega_1\tau'_K} \\ e^{-j\omega_3\tau'_1} & \cdots & e^{-j\omega_3\tau'_K} \\ \vdots & \ddots & \vdots \\ e^{-j\omega_{N-1}\tau'_1} & \cdots & e^{-j\omega_{N-1}\tau'_K} \end{bmatrix} \begin{bmatrix} g_1(t) \\ \vdots \\ g_K(t) \end{bmatrix} + \boldsymbol{n}'_1(t) \\
&= \boldsymbol{A}\boldsymbol{g}(t) + \boldsymbol{n}'_1(t), \tag{21}
\end{aligned}$$

$$\begin{aligned}
\boldsymbol{x}_2(t) &= \boldsymbol{A} \begin{bmatrix} e^{-j\Delta\omega\tau'_1} & \cdots & 0 \\ \vdots & \ddots & \vdots \\ 0 & \cdots & e^{-j\Delta\omega\tau'_K} \end{bmatrix} \boldsymbol{g}(t) + \boldsymbol{n}'_2(t) \\
&= \boldsymbol{A}\boldsymbol{\Phi}\boldsymbol{g}(t) + \boldsymbol{n}'_2(t), \tag{22}
\end{aligned}$$

where $\boldsymbol{x}_2(t)$ is obtained from $\boldsymbol{x}_1(t)$ through a rotation, and the diagonal matrix $\boldsymbol{\Phi}$ is the rotational invariance factor. We can see that the delay information of all dynamic reflection paths are involved in $\boldsymbol{\Phi}$. Constructing equations to solve $\boldsymbol{\Phi}$, we can obtain the estimations of delays.

Concatenating $\boldsymbol{x}_1(t)$ and $\boldsymbol{x}_2(t)$, we obtain a new vector

$$\begin{aligned}
\boldsymbol{y}(t) &= \begin{bmatrix} \boldsymbol{x}_1(t) \\ \boldsymbol{x}_2(t) \end{bmatrix} = \begin{bmatrix} \boldsymbol{A}\boldsymbol{g}(t) + \boldsymbol{n}'_1(t) \\ \boldsymbol{A}\boldsymbol{\Phi}\boldsymbol{g}(t) + \boldsymbol{n}'_2(t) \end{bmatrix} \\
&= \begin{bmatrix} \boldsymbol{A} \\ \boldsymbol{A}\boldsymbol{\Phi} \end{bmatrix} \boldsymbol{g}(t) + \begin{bmatrix} \boldsymbol{n}'_1(t) \\ \boldsymbol{n}'_2(t) \end{bmatrix} = \overline{\boldsymbol{A}}\boldsymbol{g}(t) + \boldsymbol{z}(t), \tag{23}
\end{aligned}$$

where the covariance matrix of $z(t)$ is $\mathbf{\Gamma}_z$. Note that $z(t)$ is a rearranged version of $n'(t)$, so that $\mathbf{\Gamma}_z$ is not equal to $\mathbf{\Gamma}$.

Then we can obtain the covariance matrix of $y(t)$,

$$
\begin{aligned}
\mathbf{R} &= E\left\{ y(t)y^H(t) \right\} \\
&= E\left\{ \overline{A}g(t)g^H(t)\overline{A}^H + z(t)z^H(t) \right\} \\
&= \overline{A}E\left\{ g(t)g^H(t) \right\}\overline{A}^H + E\left\{ z(t)z^H(t) \right\} \\
&= \overline{A}R_s\overline{A}^H + \mathbf{\Gamma}_z.
\end{aligned}
\tag{24}
$$

Calculate the generalized eigendecomposition of the matrix pair $(\mathbf{R}, \mathbf{\Gamma}_z)$,

$$
\mathbf{R}U = \mathbf{\Gamma}_z U\mathbf{\Lambda},
\tag{25}
$$

where U is the generalized eigen space, $\mathbf{\Lambda} = diag\{\lambda_1, \ldots, \lambda_N\}$ are generalized eigenvalues. Since there are K dynamic paths, the first K eigenvalues should be significantly larger than the latter $N - K$ eigenvalues.

The eigen space U can thus be separated into signal subspace U_s and null space U_n, i.e.,

$$
U = [U_s, U_n],
\tag{26}
$$

where U_s is the former K columns of U, and U_n is the latter $N - K$ columns of U. The subspace spanned by $\mathbf{\Gamma}_z U_s$ should be consisted with the subspace spanned by $\overline{A}$. Thus there must exist one non-singular matrix T, so that

$$
U'_s = \mathbf{\Gamma}_z U_s = \overline{A}T.
\tag{27}
$$

Separating U'_s into upper and lower half matrices, we can get

$$
U'_s = \begin{bmatrix} U_1 \\ U_2 \end{bmatrix} = \begin{bmatrix} A \\ A\mathbf{\Phi} \end{bmatrix}T.
\tag{28}
$$

Thereafter, we can derive that

$$
U_2 = A\mathbf{\Phi}T = U_1 T^{-1}\mathbf{\Phi}T = U_1\mathbf{\Psi},
\tag{29}
$$

where $\mathbf{\Psi} = T^{-1}\mathbf{\Phi}T$. The eigenvalues of $\mathbf{\Psi}$ must be equal to the diagonal elements of $\mathbf{\Phi}$, and the columns of T are the eigenvectors of $\mathbf{\Psi}$. Through solving $\mathbf{\Psi}$, we can get rotational factor $\mathbf{\Phi}$, and then get the delay estimation.

The standard least-squares (LS) solution of $\mathbf{\Psi}$ is

$$
\mathbf{\Psi} = (U_1^H U_1)^{-1}U_1^H U_2.
\tag{30}
$$

However, in practical systems the covariance matrix $\mathbf{R}$ is obtained from a finite number of noisy measurements, and thus there are errors in the estimation of $\mathbf{R}$ and its eigenvectors. With probability one, the spanned space of U'_s is not exactly overlapped with the spanned space of $\overline{A}$. In other words, both U_1 and U_2 are noisy. In this situation, the total least-squares (TLS) criterion is preferred to calculate $\mathbf{\Psi}$.

Calculate the eigenvalue decomposition,

$$
\begin{bmatrix} U_1^H \\ U_2^H \end{bmatrix}[U_1 U_2] = E\mathbf{\Lambda}_E E^H,
\tag{31}
$$

and partition E into $K \times K$ submatrices,

$$
E = \begin{bmatrix} E_{11} & E_{12} \\ E_{21} & E_{22} \end{bmatrix}.
\tag{32}
$$

The TLS solution of $\mathbf{\Psi}$ is

$$
\mathbf{\Psi} = -E_{12}E_{22}^{-1}.
\tag{33}
$$

C. DELAY ESTIMATION OF STATIC PATHS

In this part, we try to estimate the delay of the direct path. Although in many situations, like in indoor or urban environments, densely scattering is present, we are focusing on the direct path and specular reflections. In a short duration, the amplitudes and phases of static paths are all keep fixed. These static paths contribute to the static channel response. Thus unlike the estimation of dynamic paths, the frequency-domain channel response vector of static paths will span a one-dimensional subspace, no matter how many static reflection existed. The subspace-based super-resolution algorithms are no longer applicable here. To solve this problem, we consider two optimization based methods. With the known frequency-domain channel response of the given delay (i.e., pulse waveform in time-domain), we are looking for the amplitude, phase and delay of each path to fit the overall superimposed channel response.

1) DELAY ESTIMATION BASED ON SPARSE OPTIMIZATION

We consider time delay estimation problem of the static paths in frequency domain. The frequency-domain channel response is the summation of channel responses of the L static paths,

$$
\hat{H}_s(\omega) = \sum_{l=1}^{L} a_l e^{-j\omega_c \tau_l} e^{-j\omega\tau'_l} + n_s(\omega),
\tag{34}
$$

and the channel responses in different baseband frequency can form a vector

$$
\hat{h}_s = \begin{bmatrix} \hat{H}_s(\omega_1) & \hat{H}_s(\omega_2) & \cdots & \hat{H}_s(\omega_N) \end{bmatrix}^T.
\tag{35}
$$

The delay estimation problem can be modeled as a sparse optimization problem, which is to find the position of those distinct paths.

Define a dictionary $\mathbf{D} \in \mathbb{C}^{N \times F}$, in which different atoms correspond the channel responses with different delays. Then the delay estimation problem can be formulated as a sparse optimization problem, i.e.,

$$
\boldsymbol{\alpha} = \arg\min_{\boldsymbol{\alpha}} \left\{ \frac{1}{2}\|\hat{h}_s - \mathbf{D}\boldsymbol{\alpha}\|_2^2 + \|\boldsymbol{\alpha}\|_1 \right\},
\tag{36}
$$

where the element of $\boldsymbol{\alpha}$ is the weight of the channel response with different delay. The first term of the right side is to minimize the fitting error, i.e., to fit the static channel response with weighted sum of the channel responses with different delay. The second term is to minimize the L_1 norm of the weighting vector $\boldsymbol{\alpha}$. Optimizing the L_1 norm is an approximation of the optimizing of L_0 norm, which is to minimize the number of non-zero elements in $\boldsymbol{\alpha}$. To minimize the sum

TABLE 1. OMP based delay estimation.

Initialize the residual error $\varepsilon_0 = \hat{h}_s$, and the sparse matrix $X_0 = \emptyset$.

repeat
1. Find the atom that has the highest correlation with the residual error,
   $d_i^* = \arg \max |\langle \varepsilon_{i-1}, d_i \rangle|$;
2. Update sparse matrix $X_i = [X_{i-1}, d_i^*]$, and calculate the weighting vector with the LS criterion, $w^* = \arg \min \|\hat{h}_s - X_i w\|_2$;
3. Update the residual error $\varepsilon_i = \hat{h}_s - X_i w^*$.

until convergence

---

of these two terms can achieve a balance between the fitting error and the sparsity of the estimated reflection paths.

The optimization result is a sparse vector $\boldsymbol{\alpha}$ with few non-zero elements, where the positions of these non-zero elements represent the delay estimations of the static reflection paths, and the weights represent the amplitudes and phases of them. Although we only require the delay of the first arrived path, we can not get this parameter alone without joint estimation of other information.

The problem (36) is a convex optimization problem, which can be solved by some standard optimization program, such as CVX. But the computational burden is high, and it is not appropriate for realtime processing.

2) DELAY ESTIMATION BASED ON ORTHOGONAL MATCHING PURSUIT

To reduce the computational burden, we consider a simpler delay estimation algorithm based on orthogonal matching pursuit (OMP). OMP is an sparse representation algorithm by orthogonal decomposition. It uses sparse combinations from a complete dictionary, and to synthesize the original signal iteratively through fitting the residual error. The OMP algorithm will orthogonalize the atoms at every decomposition step, this will greatly increase the convergence speed.

The basic procedure is as follows. First, we construct the dictionary of channel response vectors, where each vector corresponds to a possible delay. Then we look for the dictionary atom which has the highest correlation with the overall static channel response, and calculate the weight of the selected atom according to the LS criterion. Next, we calculate the residual error, look for the dictionary atom which has the highest correlation with the residual error, and update the sparse matrix with the combination of previous determined atoms and this new atom. Recalculate the weight vector and update the residual error. The iteration stops when the residual error is less than a threshold.

The detailed implementation steps of the OMP algorithm are summarized in Table 1.

IV. SIMULATION AND PERFORMANCE ANALYSIS

In this section, we will first derive the Cramer-Rao lower bound (CRLB) of the delay estimation problem, and analyze the relationship between the estimation error and various parameters, e.g., SNR, signal bandwidth, delay differences. Then we will simulate the performance of the delay estimation methods under various configurations and compare with CRLB.

A. CRAMER-RAO LOWER BOUND

According to (17)-(20), if there are K dynamic reflection paths, the frequency-domain channel response vector at time t is expressed as

$$\hat{h}_d(t) = h_d'(t) + n'(t)$$

$$= \sum_{i=1}^K \alpha_i e^{-j\varphi_i(t)} \left[e^{-j\omega_1 \tau_i'}, \cdots, e^{-j\omega_M \tau_i'} \right]^T + n'(t), \quad (37)$$

where $n'(t)$ is the noise and interference vector at time t, and the covariance matrix of $n'(t)$ is Γ.

The CRLB is given by the inverse of the Fisher information matrix (FIM), i.e.,

$$P_{cr} = FIM^{-1}, \quad (38)$$

where the element of FIM is

$$FIM_{k,p} = 2 \sum_{t=1}^N Re \left\{ \left(\frac{\partial h_d'(t)}{\partial \tau_k'} \right)^H \Gamma^{-1} \left(\frac{\partial h_d'(t)}{\partial \tau_p'} \right) \right\}. \quad (39)$$

If there is only circular symmetric white Gaussian noise in $n'(t)$, $\Gamma = \sigma^2 I$. When $k = p$,

$$FIM_{k,k} = \frac{2}{\sigma^2} \sum_{t=1}^N Re \left\{ \left(\frac{\partial h_d'(t)}{\partial \tau_k'} \right)^H \left(\frac{\partial h_d'(t)}{\partial \tau_k'} \right) \right\}$$

$$= \frac{2N}{\sigma^2} \alpha_k^2 \sum_{i=1}^M \omega_i^2. \quad (40)$$

When $k \neq p$,

$$FIM_{k,p} = \frac{2}{\sigma^2} \sum_{t=1}^N Re \left\{ \left(\frac{\partial h_d'(t)}{\partial \tau_k'} \right)^H \left(\frac{\partial h_d'(t)}{\partial \tau_p'} \right) \right\}$$

$$= \frac{2}{\sigma^2} \sum_{t=1}^N Re \left\{ \alpha_k \alpha_p e^{-j[\varphi_k(t) - \varphi_p(t)]} \sum_{i=1}^M \omega_i^2 e^{-j\omega_i(\tau_k' - \tau_p')} \right\}. \quad (41)$$

Discussion: From (40) and (41) we can see that, $FIM_{k,k}$ is proportional to the integration time N and the SNR of the reflection path α_k^2/σ^2. With larger bandwidth, $FIM_{k,k}$ will also increase with ω_M. If there is only one path, the CRLB of the delay estimation τ_k is the inverse of $FIM_{k,k}$. Thus larger $FIM_{k,k}$ implies lower estimation error.

If there are multiple paths, the difference of the delays will affect the value of $FIM_{k,p}$, and then affect the value of P_{cr}. For example, if $\tau_k' - \tau_p' = 2\pi/\omega_M$, the summation term $\sum_{i=1}^M \omega_i^2 e^{-j\omega_i(\tau_k' - \tau_p')}$ will be close to zero, thus $FIM_{k,p}$ is close to zero. On the contrary, if the delays of two paths are very close, i.e., $\tau_k' - \tau_p' \approx 0$, the value of $FIM_{k,p}$ will further depends on $\varphi_k(t) - \varphi_p(t)$. If the phase difference $\varphi_k(t) - \varphi_p(t)$ keeps changing, the summation items inside the brace will cancel each other out. The worst case is that $\varphi_k(t) - \varphi_p(t)$ keeps unchanged for $t = 1$ to N, then $FIM_{k,p}$ is close to $FIM_{k,k}$, this will decrease the determinant of FIM and increase the CRLB.

TABLE 2. Simulation parameters.

Signal Format	LTE	Carrier Frequency	2.3 GHz
Subcarrier Space	90 KHz	Subcarrier Number	200
Tx Position	(0, 0) m	Rx Position	(10, 0) m
Target Origination	(5, 10) m	Moving Speed	(1, 1.5) m/s

If there is also interference caused by the residual phase noise in $n'(t)$, as shown in (19) and (20), the correlation between $h_d'(t)$ and $h_s'(t)$ will also affect the values of FIM. If their correlation is high, the determinant of *FIM* will be small and this will also increase the CRLB.

The CRLB of the estimation error of the static paths can be similarly derived. Since the SNR of the static path is much higher than that of the dynamic paths, the CRLB of the delay estimation of the static paths should be much lower.

B. SIMULATION RESULTS

We first consider the situation that only one moving object exists. The root mean square error (RMSE) of the delay estimation of the dynamic path is simulated, and the corresponding CRLB is calculated. The simulation parameters are listed in Table 2. We assume the LTE signal is transmitted at 2.3 GHz center frequency. The frequency interval between CRS subcarriers is 90 KHz, and totally 200 CRS subcarriers are used, which is the typical configuration in 20MHz bandwidth LTE signals.

The position of the transmitter is at (0, 0) m, and the position of the receiver is at (10, 0) m. The start position of the moving target is at (5, 10) m, and its moving speed is (1, 1.5) m/s. We fix the ratio of the direct path power and the reflection path power as 10 dB, and change the SNR of the reflection path power to the white Gaussian noise. The CSI is obtained from the physical layer every 1 ms, and the integration time of the covariance matrix for each estimation is 100 ms. The delay estimation performance of the ESPRIT algorithm and the CRLB are shown in Fig. 3. For the convenience of readers, the RMSE of delay estimation is multiplied by the light speed, so that the unit of measurement error is transformed to meter.

From Fig. 3 we can see that, in logarithm scale the CRLB is inversely proportional to the SNR. It is well known that the ESPRIT algorithm has threshold effect, its performance gets bad seriously when the SNR is lower than a threshold. We can clearly see this point in Fig. 3. For the estimation algorithm with full paths (using all paths in time domain), when the SNR is lower than -15 dB, the performance will dramatically degrade. We also tested the performance of an estimation algorithm using extracted paths, where the frequency domain channel response is first transformed into time domain, and then a 7 samples long window is applied on the channel response to extract the main paths and set the values of other paths as zeros. We hope this method can suppress noise, and we do observe the performance improvement in lower
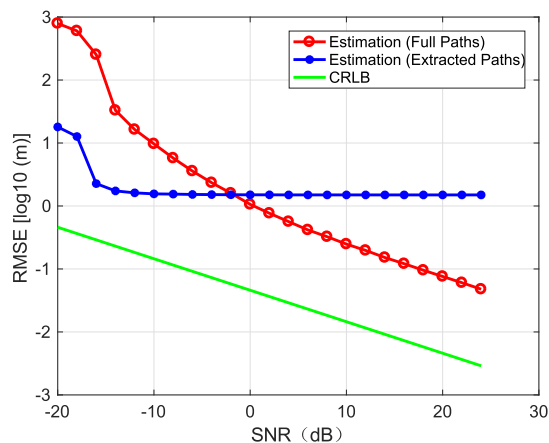

FIGURE 3. RMSE of the distance estimation of one target with different SNRs.
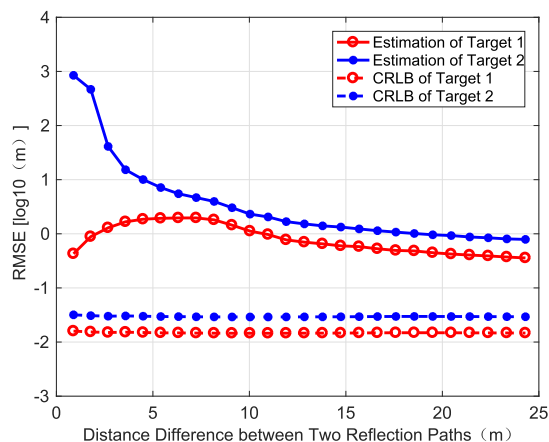

FIGURE 4. RMSE of the distance estimations of two targets with different distance intervals.

SNR region. But in high SNR region, the performance of this method degrades, and it has an error floor. This phenomenon is because the pulse shape of the transmitted signal is not an ideal impulse, it actually has many side lobes. When we extract the main paths, the information hidden in side lobes will be lost. This will certainly cause extra estimation error.

Next, we consider the situation where there are two moving objects simultaneously existed in the environment. From the derivation of CRLB, we know that the delay difference of two paths will affect the performance of the delay estimation. Thus in this simulation, we change the distance difference of these two reflection paths, and the other parameters are keeping fixed. The SNRs of the direct path, the first reflection path, and the second reflection path is 20 dB, 10 dB, and 3 dB, respectively. The estimation errors and CRLBs of these two paths are shown in Fig. 4.

From Fig. 4 we can see that, for target 2 the estimation error decreases monotonically along with the increasing of the distance difference of the two reflection paths. However, for target 1 the estimation error increases first and only turns down to decrease after the distance difference grows larger than 7.5 m. Since the first reflection path is stronger than
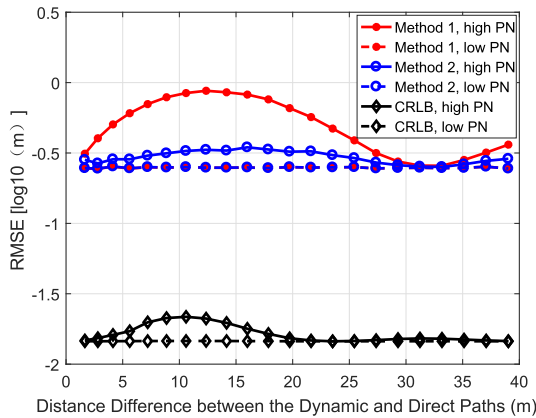
FIGURE 5. RMSE of the distance estimation with the impact of phase noise.

FIGURE 6. RMSE of the distance estimation of the direct path.

the second reflection path, when these two paths are too close, the ESPRIT algorithm cannot distinguish two paths, and only the delay of the stronger path is estimated. Thus in this situation the estimation error of the first path is small, but the estimation error of the second path is very large. When the two paths separate a while, the ESPRIT algorithm can distinguish two paths, but they will cause interference to each other, thus the estimation errors of both paths are large. Until after their separation is larger than half of the pulse width, both estimation errors begin to decrease simultaneously.

In practical system, the residual phase noise will cause interference due to the residual static channel response. Fig. 5 shows its impact on the estimation error with two situations. One is that the variance of residual phase noise is larger than the variance of the Gaussian noise, i.e., $\sigma_\phi^2 = 10\sigma^2$. The other is opposite, $\sigma_\phi^2 = 0.1\sigma^2$. Since the residual static channel response will cause interference to the estimation of the delay of the dynamic path, the delay difference between the dynamic path and the static path will affect the performance. In this simulation, there is only one moving target, and the SNRs of the direct path and the reflection path are 20 dB and 10 dB, respectively.

For both of the high phase noise (high PN) and low phase noise (low PN) situations, we have tried two estimation methods. The first one (Method 1) only considers the variance of Gaussian noise in the covariance matrix of $\boldsymbol{n}'(t)$, as in (20), even that the residual phase noise is actually existed. The second one (Method 2) considers both the impact of Gaussian noise and the residual phase noise. We can see from Fig. 5 that when the residual phase noise is small, the estimation error is mainly affected by the Gaussian noise, both methods have similar performance and we cannot see any variation when the delay between the dynamic path and static path changes. However, when the residual phase noise is large, it will cause obvious influence. The RMSE of the delay estimation changes with the distance difference of the dynamic and direct paths. Moreover, the variation of the first method is much larger than that of the second method, means that the estimation performance will be greatly impacted if we neglect the effect of the residual phase noise.
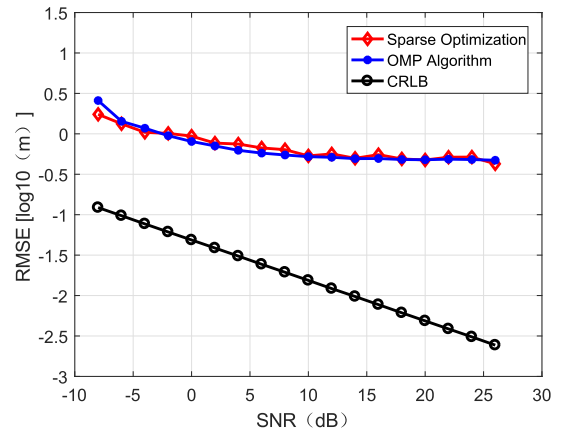
At last, let us see the delay estimation performance of the static paths. We consider that there are three static paths in the channel, including one direct path and two reflection paths. The delays of them are randomly set in (0, 100) ns, and the first arrived path is always the direct path. The amplitude ratios of these three paths are set as 1 : 0.1 : 0.02. The RMSE of the delay estimation and the corresponding CRLB are shown in Fig. 6, where the shown SNR is defined as the SNR of the direct path. We can see that the RMSE decreases with the increasing of SNR. The CRLB is quite low when SNR is greater than 25 dB, say less than 0.01 m. But the performance of the sparse optimization and the OMP algorithm are not as good as the bound. It seems that there is an error floor, which cannot be further reduced even if we reduce the interval of the atoms in the dictionary. Since the OMP algorithm has lower computational complexity than the sparse optimization algorithm, and their performance are similar, we will use the OMP algorithm to estimation the delay of the static paths in the following experiments.

V. PROTOTYPE IMPLEMENTATION AND EXPERIMENT RESULTS

A. PROTOTYPE AND MEASUREMENT ENVIRONMENTS

We designed a prototype system to receive LTE signals. The RF part is implemented on AD-FMCOMMS2, which is an evaluation board of the RF transceiver chip AD9361. AD9361 is a popular RF chip used in 4G base stations, it has adjustable carrier frequency from 70 MHz to 6 GHz. The baseband processing is on ZedBoard, an evaluation board of the Xilinx all programmable SoC chip Zynq-7020. Zynq-7020 involves dual-core ARM processors and programmable logics, so we can implement our own baseband processing algorithms on chip. To reduce the implementation complexity and get real-time results, for each subframe of LTE signal we only extract one time of channel estimation. This is equivalent to 1 ms sampling interval to the channel response.

We use another prototype to transmit LTE signal, so that the measurement environment is under control. The transmit power is 10 dBmW and the carrier frequency is 2.3 GHz.

FIGURE 7. The experiment environment.

FIGURE 8. The geometric configuration of test scenes.

As a comparison, the transmit power of a real macro-BS is about 46 dBmW, and that of a micro-BS is about 30 dBmW. We implement the experiments in the hall of a building, as shown in Fig. 7, where there are plenty of static reflections by the walls and facilities. We use a transmitter with one transmit antenna, and a receiver with two receiving antennas. The receiver can simultaneously processes two incoming signals from two antennas, thus for the convenience of description we just call that there are two receivers. The positions of the transmitter and receivers are as shown in Fig. 8, two receivers are located on both sides of the right triangle while the transmitter is at the origin of the coordinate. There is LOS propagation between the transmitter and receiver, and their distance is set as 4 m. If we use power amplifier on the transmitter side, the distance of the measurement environment can be correspondingly enlarged. But as we have clarified, the error of delay estimation depends on the SNR instead of the propagation distance. This configuration is just an example to show the performance of the proposed schemes. In practical situations, we can use one receiver to receive the signals from multiple surrounding base stations. This will fully use the opportunity provided by the signals over the air.

A walking human is tested as the moving object, whose RCS is about 0.5 m^2, and the relative permittivity of the clothes is about 5. We tested two traces to see the delay estimation and localization results. As shown in Fig. 8, the first trace is along the diagonal line of the triangle, from (7, 7) m to (1.4, 1.4) m, the total moving distance is 8 m. The other trace is on the arc with radius 8 m, the coverage angle is about $\pi/3$ and the total moving distance is also 8 m. The walking speed is about 1.6 m/s.

B. SIGNAL WAVEFORMS AND THE EIGENVALUES

Let us first see the channel response when the human is moving on trace 1. To see the time-variant effect clearly, we transformed the channel response from frequency domain to time domain, and only see the 7 samples around the main path. From Fig. 9, we can see that when the human is far away from the transmitter and receiver, the reflection path is weak,
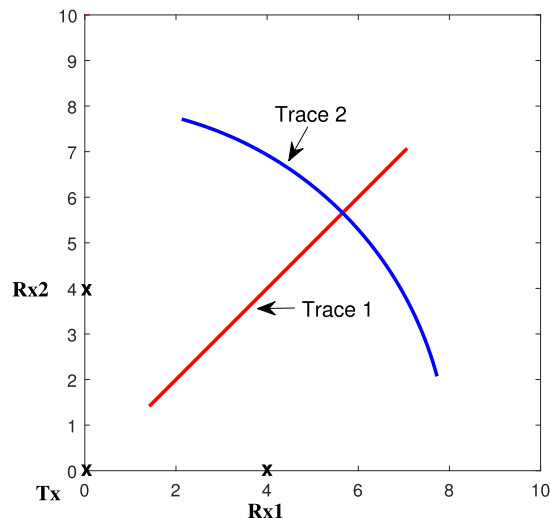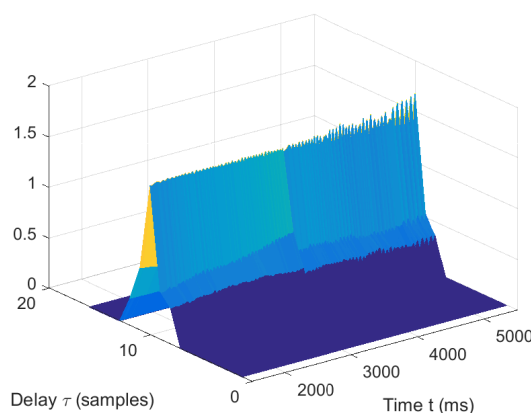

FIGURE 9. The time-domain channel response.

and the ripples caused by the interference between the direct path and the reflection path is not obvious. On the contrary, when the human moves close, the reflection path becomes strong and the ripples becomes significant.

The overall channel response is the superposition of the static paths and the dynamic paths. If we separate the dynamic paths from the static paths, the variation of the channel response will be clearer. Fig. 10 shows the real and imaginary parts of the separated dynamic channel response, where only the main path in time domain is demonstrated. We can see that when the reflection path is weak, the noise variance in the imaginary part is larger than that in the real part. This is actually the impact of the residual phase noise. As we have derived in (16), the residual phase noise mainly affect the imaginary part of the dynamic channel response.

With the dynamic channel response, we can form the covariance matrix R as in (24). Fig. 11 shows the eigenvalues of R, and Fig. 12 shows the generalized eigenvalues of matrix pair (R, Γ_z), where the y-axis is in logarithm values. The first and second largest eigenvalues are shown. In this experiment, the human moving actually starts at 1.5 second and stops
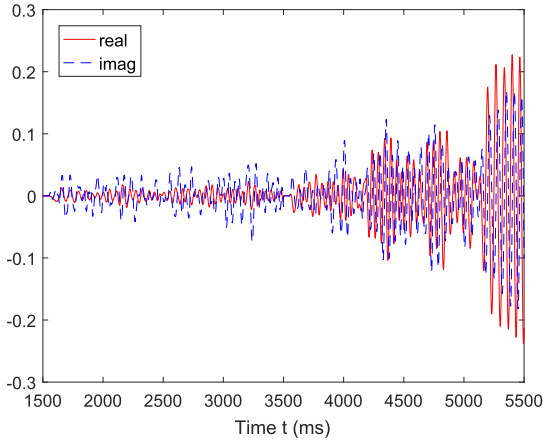
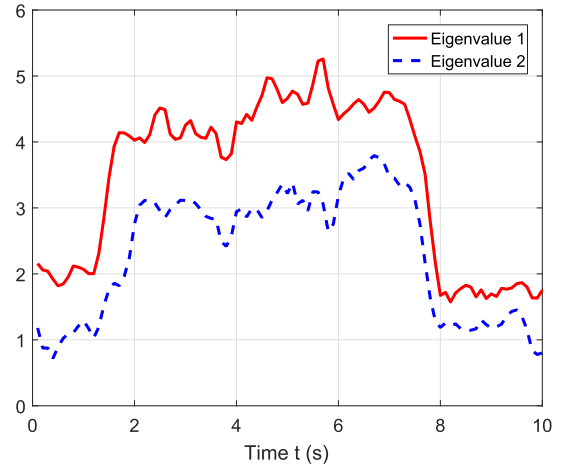**FIGURE 10.** The real and imaginary parts of the dynamic channel response.

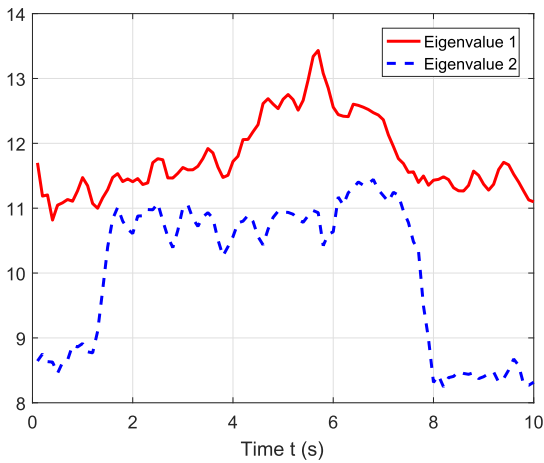**FIGURE 12.** The first and second largest generalized eigenvalues of (R, Γ_z).

FIGURE 11. The first and second largest eigenvalues of R.
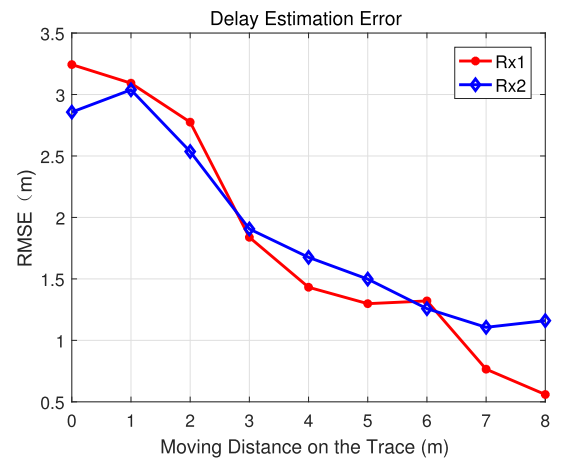

FIGURE 13. The RMSE of delay estimations on trace 1.

at 7.5 second. We can see that the eigenvalues change with the moving states and the reflective strength. In Fig. 11, when the human is not moving (before 1.5s and after 7.5s), the first largest eigenvalue is coming from Γ_z, i.e., the interference caused by static paths and the residual phase noise, and the second largest eigenvalue is coming from the Gaussian noise. When the human is moving, depending on the strength of the reflection path, the first largest eigenvalue might be caused by the interference or by the dynamic path. Thus if we only use the eigenvalues of R, there might be mistake to choose the expected signal subspace corresponds to the dynamic path. On the contrary, in Fig. 12 we can see that the largest generalized eigenvalue only corresponds to the dynamic path. We can always choose the correct subspace based on the largest eigenvalue.

C. DELAY ESTIMATION AND LOCALIZATION RESULTS

The root mean square error (RMSE) of delay estimation results are given in Fig. 13, where the human is moving on trace 1. For the convenience of comparing, the delay estimation results are multiplied with the light speed, i.e., the

values we actually demonstrated are the estimation error of propagation distances. For each trace, we have repeated the experiment for 20 times, and then the statistical results are calculated. Fig. 14 shows the RMSE of the localization results by using the delay estimations from Rx1 and Rx2. We can see that when the human is at the far end of the trace, the delay estimation error is large and thus the localization error is large. While when the human moves close to the near end, the delay estimation error reduces and correspondingly the localization performance improves. The reflection path is weaker when the propagation distance is longer, and the performance of delay estimation is greatly affected by the SNR of the reflection path.

The performance of delay estimation and localization on trace 2 are shown in Fig. 15 and 16. We can see that the estimation error is larger in this case. The main reason is that, on trace 2 the variation of carrier phase is much slower. It is only about 1/5 of the variation speed on trace 1. Although the moving speed of the human is the same, the propagation distance of the reflection path changes with different rates
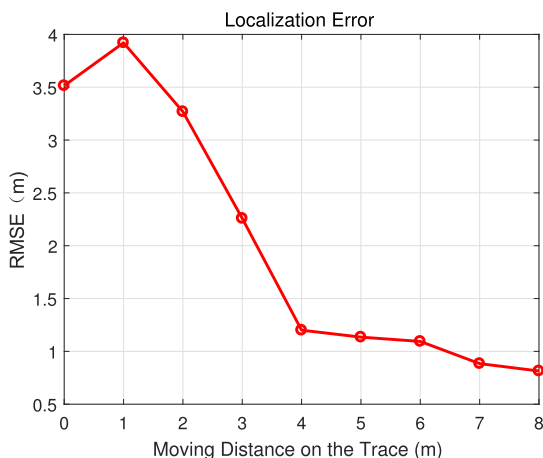
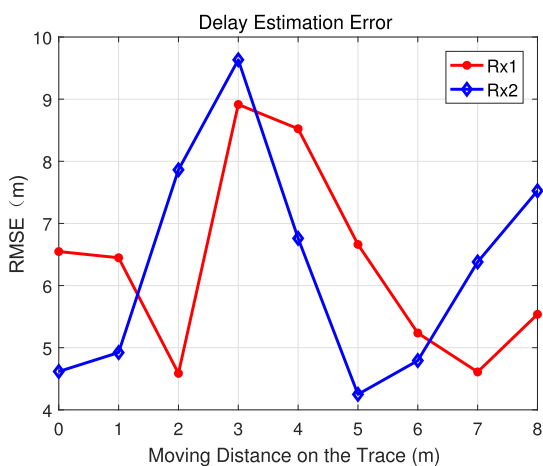**FIGURE 14.** The RMSE of localization results on trace 1.

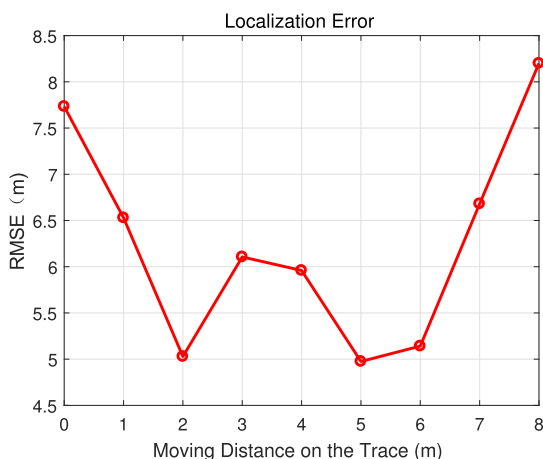**FIGURE 15.** The RMSE of delay estimations on trace 2.

FIGURE 16. The RMSE of localization results on trace 2.

given different geometry configurations. The slower changing carrier phase will affect the covariance estimation of the dynamic channel vector, and then affect the estimation error of the ESPRIT algorithm.

VI. CONCLUSION

In this paper, a passive localization method using the opportunistic on-the-air LTE signal is studied. We built a channel model that incorporate the transceiver imperfections, and the impacts of timing drift and phase noise are specially emphasized. Then we designed the preprocessing method to separate the dynamic and static channel responses, and proposed corresponding delay estimation methods for the dynamic and static paths. The CRLB of the delay estimation problem is derived, and simulations are executed to analyze the impacting factors. A prototype is implemented and passive localization experiments are carried out in real environments. The experiment results show the preliminary feasibility of passive localization via on-the-air LTE signals, and the performance is mainly restricted by weak reflection and slow movement.

REFERENCES

[1] Y. Tian, H. Duan, and Y. He, "Passive localization via on-the-air LTE signals," in *Proc. 7th IEEE ICC Workshop*, May 2019, pp. 1–6.

[2] P. M. Holl and F. Reinhard, "Holography of Wi-Fi radiation," *Phys. Rev. Lett.*, vol. 118, no. 18, May 2017, Art. no. 183901.

[3] B. Wang, Q. Xu, C. Chen, F. Zhang, and K. J. R. Liu, "The promise of radio analytics: A future paradigm of wireless positioning, tracking, and sensing," *IEEE Signal Process. Mag.*, vol. 35, no. 3, pp. 59–80, May 2018.

[4] J. Lien, N. Gillian, M. E. Karagozler, P. Amihood, C. Schwesig, E. Olson, H. Raja, and I. Poupyrev, "Soli: Ubiquitous gesture sensing with millimeter wave radar," *ACM Trans. Graph.*, vol. 35, no. 4, p. 142, Jul. 2016.

[5] K. Witrisal, P. Meissner, E. Leitinger, Y. Shen, C. Gustafson, F. Tufvesson, K. Haneda, D. Dardari, A. F. Molisch, A. Conti, and M. Z. Win, "High-accuracy localization for assisted living: 5G systems will turn multipath channels from foe to friend," *IEEE Signal Process. Mag.*, vol. 33, no. 2, pp. 59–70, Mar. 2016.

[6] L. Yang, Y. Chen, X.-Y. Li, C. Xiao, M. Li, and Y. Liu, "Tagoram: Real-time tracking of mobile RFID tags to high precision using cots devices," in *Proc. ACM MobiCom*, Sep. 2014, pp. 237–248.

[7] C. Hu, C. Liu, R. Wang, L. Wang, and L. Chen, "Detection and SISAR imaging of aircrafts using GNSS forward scatter radar: Signal modeling and experimental validation," *IEEE Trans. Aerosp. Electron. Syst.*, vol. 53, no. 4, pp. 2077–2093, Aug. 2017.

[8] D. Halperin, W. Hu, A. Sheth, and D. Wetherall, "Tool release: Gathering 802.11n traces with channel state information," *ACM SIGCOMM Comput. Commun. Rev.*, vol. 41, no. 1, p. 53, Jan. 2011.

[9] Q. Pu, S. Gupta, S. Gollakota, and S. Patel, "Whole-home gesture recognition using wireless signals," in *Proc. ACM MOBICOM*, Sep. 2013, pp. 27–38.

[10] G. Wang, Y. Zou, Z. Zhou, K. Wu, and L. M. Ni, "We can hear you with Wi-Fi!" *IEEE Trans. Mobile Comput.*, vol. 15, no. 11, pp. 2907–2920, Nov. 2016.

[11] H. Wang, D. Zhang, Y. Wang, J. Ma, Y. Wang, and S. Li, "RT-Fall: A real-time and contactless fall detection system with commodity WiFi devices," *IEEE Trans. Mobile Comput.*, vol. 16, no. 2, pp. 511–526, Feb. 2017.

[12] D. Zhang, Y. Hu, Y. Chen, and B. Zeng, "BreathTrack: Tracking indoor human breath status via commodity WiFi," *IEEE Internet Things J.*, vol. 6, no. 2, pp. 3899–3911, Apr. 2019.

[13] J. Wang, Y. Zhao, X. Fan, Q. Gao, X. Ma, and H. Wang, "Device-free identification using intrinsic CSI features," *IEEE Trans. Veh. Technol.*, vol. 67, no. 9, pp. 8571–8581, Sep. 2018.

[14] C. Wu, Z. Yang, Z. Zhou, X. Liu, Y. Liu, and J. Cao, "Non-invasive detection of moving and stationary human with WiFi," *IEEE J. Sel. Areas Commun.*, vol. 33, no. 11, pp. 2329–2342, Nov. 2015.

[15] K. Qian, C. Wu, Z. Yang, Y. Liu, F. He, and T. Xing, "Enabling contactless detection of moving humans with dynamic speeds using CSI," *ACM Trans. Embedded Comput. Syst.*, vol. 17, no. 2, Apr. 2018, Art. no. 52.

[16] H. Zhu, F. Xiao, L. Sun, R. Wang, and P. Yang, "R-TTWD: Robust device-free through-the-wall detection of moving human with WiFi," *IEEE J. Sel. Areas Commun.*, vol. 35, no. 5, pp. 1090–1103, May 2017.

[17] M. Edrich, A. Schroeder, and F. Meyer, "Design and performance evaluation of a mature FM/DAB/DVB-T multi-illuminator passive radar system," *IET Radar, Sonar Navigat.*, vol. 8, no. 2, pp. 114–122, Feb. 2014.

[18] S. Lutz, V. Winkler, R. Müller, and C. Klöck, "Multi static long range multi band 3D passive radar—Latest developments at Hensoldt Sensors," in *Proc. 19th Int. Radar Symp. (IRS)*, Jun. 2018, pp. 1–9.

[19] Z. Zhao, X. Wan, D. Zhang, and F. Cheng, "An experimental study of HF passive bistatic radar via hybrid sky-surface wave mode," *IEEE Trans. Antennas Propag.*, vol. 61, no. 1, pp. 415–424, Jan. 2013.

[20] J. Yi, X. Wan, H. Leung, and F. Cheng, "MIMO passive radar tracking under a single frequency network," *IEEE J. Sel. Topics Signal Process.*, vol. 9, no. 8, pp. 1661–1671, Dec. 2015.

[21] C. R. Berger, B. Demissie, J. Heckenbach, P. Willett, and S. Zhou, "Signal processing for passive radar using OFDM waveforms," *IEEE J. Sel. Topics Signal Process.*, vol. 4, no. 1, pp. 226–238, Feb. 2010.

[22] J. Y. Shen and A. F. Molisch, "Estimating multiple target locations in multi-path environments," *IEEE Trans. Wireless Commun.*, vol. 13, no. 8, pp. 4547–4559, Aug. 2014.

[23] S. Aditya, A. F. Molisch, N. Rabeah, and H. M. Behairy, "Localization of multiple targets with identical radar signatures in multipath environments with correlated blocking," *IEEE Trans. Wireless Commun.*, vol. 17, no. 1, pp. 606–618, Jan. 2018.

[24] D. Zhang, H. Wang, and D. Wu, "Toward centimeter-scale human activity sensing with Wi-Fi signals," *Computer*, vol. 50, no. 1, pp. 48–57, Jan. 2017.

[25] T. S. Rappaport, *Wireless Communications: Principles and Practice*. Upper Saddle River, NJ, USA: Prentice-Hall, 1996.

[26] S. Xu and Y. Tian, "Device-free motion detection via on-the-air LTE signals," *IEEE Commun. Lett.*, vol. 22, no. 9, pp. 1934–1937, Sep. 2018.

[27] S. Bartoletti, A. Conti, and M. Z. Win, "Passive radar via LTE signals of opportunity," in *Proc. IEEE Workshop ICC*, Jun. 2014, pp. 181–185.

[28] P. Stoica and R. Moses, *Spectral Analysis of Signals*. Upper Saddle River, NJ, USA: Prentice-Hall, 2005.

YAFEI TIAN (S'05–M'08) received the B.S. degree in electronics engineering and the Ph.D. degree in signal and information processing from Beihang University, Beijing, China, in 2001 and 2008, respectively. He was a Visiting Scholar with the University of Southern California, Los Angeles, CA, USA, from 2010 to 2011. He is currently an Associate Professor with the School of Electronics and Information Engineering, Beihang University. His research interests include 5G cellular systems, MIMO precoding and interference mitigation, passive localization, and wireless sensing.

YANGYANG HE received the B.S. degree from the School of Electronics and Information Engineering, Beihang University, Beijing, China, in 2018, where he is currently pursuing the M.S. degree. His primary research interests include physical layer of 5G wireless communications, passive localization, and wireless sensing.

HAO DUAN received the B.S. degree from the School of Electronics and Information Engineering, Tianjin University, Tianjin, China, in 2016, and the M.S. degree in information and communication engineering from Beihang University, Beijing, China, in 2019. His primary research interests include wireless communication system design, MIMO precoding, and passive localization.

• • •